Giant Molecular Outflows Powered by Protostars in L1448

GRACE A. WOLF-CHASE[1,2], MARY BARSONY[3,4], AND JOANN O'LINGER[5]

Received _____; accepted _____

[1]Dept. of Astronomy & Astrophysics, University of Chicago, 5640 S. Ellis Ave., Chicago, IL 60637

[2]Adler Planetarium & Astronomy Museum, 1300 S. Lake Shore Drive, Chicago, IL 60605

[3]NSF POWRE Visiting Professor, Physics Department, Harvey Mudd College, Claremont, CA 91711

[4]NSF CAREER Award Recipient

[5]Jet Propulsion Laboratory, 4800 Oak Grove Dr., MS 100-22, Pasadena, CA 91109

ABSTRACT

We present sensitive ($T_R^* \approx 0.1$K), large-scale ($47' \times 7'$–corresponding to 4 pc $\times$ 0.6 pc at the source) maps of the CO J=1→0 emission of the L1448 dark cloud at 55″ resolution. These maps were acquired using the On-The-Fly (OTF) capability of the NRAO[6] 12-meter telescope atop Kitt Peak in Arizona. Outflow activity is seen on parsec-scales, with blueshifted and redshifted emission lying in distinct hemispheres to the northwest and southeast, respectively, of two NH_3 cores that contain five Class 0 protostars. Careful comparison of the spatial and velocity distribution of our high-velocity CO maps with previously published optical and near-infrared images and spectra has led to the identification of four distinct CO outflows powered by the Class 0 protostars, L1448C, L1448N(A), L1448N(B), and L1448 IRS 2. We show the direct link between heretofore unknown giant, highly collimated, protostellar molecular outflows and their previously discovered, distant optical manifestations.

We find that the outflows end essentially where the surrounding cloud runs out of molecular gas, *i.e.,* at the cloud boundaries. Integrated intensity maps over different velocity intervals indicate there is significant overlap of blue- and redshifted gas, suggesting the outflows are highly inclined with respect to the

---

[6]The National Radio Astronomy Observatory is a facility of the National Science Foundation, operated under cooperative agreement by Associated Universities, Inc.

line-of-sight, although the individual outflow position angles are significantly different. This raises the possibility of outflow collisions. Barsony et al. (1998) presented compelling evidence for one such collision between the blueshifted flow associated with L1448C, and the redshifted flow associated with L1448N(A). Here we show that a collision between outflows associated with L1448N(B) and L1448 IRS 2 might explain several aspects of the observed outflow morphologies. The velocity maps also indicate that the outflows dominate the CO line cores as well as the high-velocity wings. The magnitude of the combined flow momenta, as well as the combined kinetic energy of the flows, are sufficient to disperse the 50 $M_\odot$ NH_3 cores in which the protostars are currently forming. It remains to be shown whether the combined directions of the outflow momenta, and the efficiency of momentum transfer from outflow to ambient cloud material, are sufficient for dispersal of the L1448 molecular cloud.

Subject headings: stars: formation–ISM: jets and outflows–methods: observational (On-The-Fly spectral line mapping)–ISM: individual (L1448) –ISM: kinematics and dynamics

1. Introduction

It has long been an open question whether young stars could be the agents of dispersal of their parent molecular clouds through the combined effects of their outflows (Norman & Silk 1979; Bertoldi & McKee 1996). The answer to this question is two-fold: the outflows must have the requisite kinetic energy to overcome the gravitational binding energy of the cloud and they must supply adequate momentum in both magnitude and direction to account for large-scale cloud dispersal.

For considerations of molecular cloud dispersal, addressing the question of the adequacy of outflow momenta has historically lagged behind determinations of outflow energetics. This is because evaluation of the available energy sources needed to account for the observed spectral linewidths in a cloud is adequate for quantitative estimates of outflow energies. However, in order to address whether the requisite momentum for cloud dispersal exists in a given case requires well-sampled, sensitive, large-scale mapping of sufficiently large areas to encompass entire molecular clouds. Such observing capability has been beyond reach until the last few years, with the implementation of "rapid " or "On-The-Fly" mapping capabilities at large-aperture millimeter telescopes.

The fact that many outflows powered by young stellar objects actually extend well beyond their parent molecular cloud boundaries has been recognized only recently, with the advent of large-scale, narrowband optical imaging surveys that have revealed shock-excited Herbig-Haro objects at parsec-scale separations from their exciting sources (Bally, Devine,

& Reipurth 1996a; Bally, Devine, & Alten 1996b; Bally et al. 1997; Devine et al. 1997; Eislöffel & Mundt 1997; Wilking et al. 1997; Gomez, Whitney, & Kenyon 1997; Gomez, Whitney, & Wood 1998; Reipurth, Devine, & Bally 1998) and from equally large-area, sensitive, millimeter line maps that show parsec-scale molecular outflows (Dent, Matthews, & Walter 1995; Lada & Fich 1996; Bence, Richer, & Padman 1996; Bence et al. 1998; O'Linger et al. 1999). The millimeter line maps of parsec-scale flows have been almost exclusively confined to instances of single, well-isolated cases, due to the tremendous confusion of multiple outflows in regions of clustered star formation, such as are found in NGC 1333 (Sandell & Knee 1998), ρ Oph, Serpens (White, Casali, & Eiroa 1995), or Circinus (Bally et al. 1999).

The L1448 dark cloud, with a mass of 100 $M_\odot$ over its $\sim$ 1.3 pc $\times$ 0.7 pc extent as traced by $C^{18}O$ emission, (Bachiller & Cernicharo 1986a), is part of the much more extensive (10 pc $\times$ 33 pc) Perseus molecular cloud complex, which contains $\approx 1.7 \times 10^4$ $M_\odot$, at a distance of 300 pc (Bachiller & Cernicharo 1986b). Although the dense NH_3 cores of L1448 contain only 50 $M_\odot$ distributed over a 1 pc $\times$ 0.5 pc area (Bachiller & Cernicharo 1986a; Anglada et al. 1989), they nevertheless harbor five Class 0 protostars: L1448C, L1448N(A), L1448N(B), L1448NW, and L1448 IRS 2 (Barsony et al. 1998; O'Linger et al. 1999; Eislöffel 2000).

High-velocity molecular gas in L1448 was discovered a decade ago via CO J=2$\rightarrow$1 and CO J=1$\rightarrow$0 mapping of a $\sim 2' \times 6'$ area centered on L1448C, acquired with 12″ and 20″

angular resolutions, respectively (Bachiller et al. 1990). Due to its brightness, high-velocity extent ($\pm$ 70 km s^{-1}), and symmetrically spaced CO bullets, the L1448C molecular outflow has been the object of much study, unlike the flows from its neighbors, the 7″ (in projected separation) proto-binary, L1448N(A)+L1448N(B), just 1.2′ to the north, or L1448 IRS 2, 3.7′ to the northwest (e.g., Curiel et al. 1990; Guilloteau et al. 1992; Bally, Lada, & Lane 1993; Bachiller et al. 1994; Davis et al. 1994; Bachiller et al. 1995; Dutrey, Guilloteau, & Bachiller 1997). Although outflow activity in the vicinity of the proto-binary had been reported previously, the H_2 and CO flows, driven by L1448N(A) and L1448N(B), respectively (Bachiller et al. 1990; Davis & Smith 1995), were not recognized as distinct until recently (Barsony et al. 1998). Identification of these flows was aided by noting the position angle of the low-excitation H_2 flow, centered on L1448N(A), to be distinct from the position angle of the CO flow from L1448N(B), defined by the direction of the line joining L1448N(B) with the newly discovered Herbig-Haro object, HH 196 (Bally et al. 1997).

Recent, wide-angle ($\sim$ 70′ field-of-view), narrowband optical imaging of the entire extent of the L1448 cloud has resulted in the discovery of several systems of Herbig-Haro objects, some displaced several parsecs from any exciting source (Bally et al. 1997). In order to investigate the link between high-velocity molecular gas and the newly discovered Herbig-Haro objects, as well as to study the possibility of cloud dispersal via outflows, we acquired new, sensitive, large-scale CO J=1$\rightarrow$0 maps of a substantial portion of the L1448 cloud. These new molecular line maps were acquired with the On-The-Fly (OTF) mapping technique as implemented at NRAO's 12-meter millimeter telescope atop Kitt

Peak, Arizona.

2. Observations and Data Reduction

The CO J=1→0 maps of L1448 presented in this paper were acquired using the spectral-line On-The-Fly (OTF) mapping mode of the NRAO's 12-meter telescope on 23 June 1997, UT 13^h53^m – UT 19^h25^m. We stress that the OTF technique allows the acquisition of large-area, high-sensitivity, spectral line maps with unprecedented speed and pointing accuracy. For comparison, it would have taken eight times the amount of telescope time, or nearly a week in practice, to acquire this same map using conventional, point-by-point mapping. Although OTF mapping is not a new concept, given the rigor of the position encoding that allows precise and accurate gridding of the data, the fast data recording rates that allow rapid scanning without beam smearing, and the analysis tools that are available, the 12m implementation is the most ambitious effort at OTF imaging yet.

To produce our CO maps of L1448, we observed a $47' \times 7'$ field along a position angle PA = 135°, (measured East from North), centered on the coordinates of L1448 IRS 2 ($\alpha_{1950} = 3^h\ 22^m\ 17.9^s$, $\delta_{1950} = 30°\ 34'\ 41''$). The 115 GHz beamwidth was $\approx 55''$. We scanned a total of 33 rows at a rate of $50''$/s, along PA = 135°, with a row spacing of $12.7''$. (The row spacing is determined by the optimum spatial sampling and by the scanning position angle.) We calibrated and integrated on an absolute off position ($\alpha_{1950} = 3^h\ 20^m$

00.0^s, $\delta_{1950} = 31^\circ\ 00'\ 00''$) at the start of every row. Each row took approximately one minute to scan. Each map coverage took $41 - 56$ minutes to complete. We performed six map coverages to attain an RMS in each OTF spectrum of $T_R^* \approx 0.11$ K.

A dual-channel, single-sideband SIS receiver was used for all observations. The backend consisted of 250 kHz and 500 kHz resolution filterbanks, yielding velocity resolutions of 0.65 km s^{-1} and 1.3 km s^{-1}, respectively. The filterbanks were used in parallel mode, each of the two receiver polarization channels using 256 filterbank channels. The polarization channels were subsequently averaged together to improve signal-to-noise. Only the 250 kHz resolution data were used to produce the maps presented here.

Line temperatures at the 12 m are on the T_R^* scale, and must be divided by the corrected main beam efficiency, η_m^*, to convert to the main-beam brightness temperature scale. For our very extended source, η_m^* is approximately 1.0. Since the corrected main-beam efficiency is the fraction of the forward power in the main diffraction beam relative to the total forward power in the main beam plus error beam, contribution from the error beam can make $\eta_m^* > 1.0$. At 115 GHz, the theoretical error beam width is $\approx 17'$, but the ratio of the error beam amplitude to the main beam amplitude is only 6×10^{-4}, suggesting contribution from the error beam can be ignored. We used the NRAO standard source, B5 ($\alpha_{1950} = 3^h\ 44^m\ 52.4^s$, $\delta_{1950} = 32^\circ\ 44'\ 28''$), to check absolute line temperatures.

The OTF data were reduced with the Astronomical Image Processing Software (AIPS), Version 15JUL95. AIPS tasks specific to OTF data are 'OTFUV', which converts a single

12 m OTF map (in UniPOPS SDD format) to UV (single-dish) format, and 'SDGRD', which selects random position single-dish data in AIPS UV format in a specified field of view about a specified position and projects the coordinates onto the specified coordinate system. The data are then convolved onto a grid. OTF data maps were first combined, then gridded into a data cube and baseline-subtracted. Channel maps as well as individual spectra were inspected to ensure good baseline removal and to check for scanning artifacts. Only the first and last rows scanned contained corrupted spectra and were rejected.

In addition to the OTF maps, we also acquired single-point spectra of the CO J=1→0 and ^{13} CO J=1→0 transitions at four individual map points. These data were used to help determine the appropriate velocity intervals for blue- and redshifted outflow emission, to determine velocity-intervals free of line emission for baseline-subtraction of the gridded OTF data, and to check CO optical depths in the line wings.

3. Results

3.1. The Extent of High-Velocity CO in L1448

Figure 1(a) shows the extent of high-velocity blue- and redshifted CO J=1→0 emission found within our OTF map boundaries, outlined by the zig-zag lines. The red contours represent high-velocity redshifted emission integrated over the velocity interval 8.1 km s^{-1} $\leq$ V_{LSR} $\leq$ 17.8 km s^{-1}, whereas the blue contours represent high-velocity blueshifted emission integrated over -12.1 km s^{-1} $\leq$ V_{LSR} $\leq$ -1 km s^{-1}. The cloud rest velocity in

the L1448 NH_3 core is V_{LSR} = 4.7 km s^{-1} for the core containing L1448C, L1448N(A), L1448N(B), and L1448NW, and V_{LSR} = 4.2 km s^{-1} for the core containing L1448 IRS 2 (Bachiller & Cernicharo 1986a). The mapped area comprises 47′ × 7′, corresponding to 4 pc × 0.6 pc at the source, at a distance of 300 pc. Stars indicate the positions of the known Class 0 sources in L1448, which include L1448C, L1448N (the unresolved, 7″ separation proto-binary L1448N(A) + L1448N(B)), L1448NW (20″ NW of the protobinary), and L1448 IRS 2, at map center. A filled square indicates the position of the Class I YSO, L1448 IRS 1 (Cohen 1980; Eislöffel 2000). Crosses indicate the positions of the known Herbig-Haro objects. Figure 1(b), the inset to Figure 1(a), shows the scale of the previously mapped region of high-velocity CO, for comparison (from Bachiller et al. 1990). This earlier map includes only a small portion of the high-velocity gas associated with Class 0 protostars in L1448. Comparison of Figures 1(a) and 1(b) highlights the truly spectacular spatial extent of outflow activity in L1448.

Several striking features are evident in Figure 1. (1) There is a ∼15′ long blueshifted filament that is connected to both the L1448N/L1448C region and to L1448 IRS 2 in a wishbone-shaped structure. This structure contains HH 197, HH 195A–D, HH 196, and culminates in HH 193. (2) There is extended redshifted outflow emission which suggests structure along three separate axes (at PAs∼129°, 150°, & 180°) directly to the southeast of L1448N/L1448C. (3) There are blueshifted and redshifted peaks in the immediate vicinity of IRS 2. The blueshifted gas peaks on HH 195E. The center of the red peak is along a line drawn through IRS 2 and HH 195A–D, on the opposite side of IRS 2. (4)

There is redshifted emission that peaks $\sim 9'$ to the southeast of IRS 2. This emission lies on a line which, if extended to the northwest of IRS 2, passes through IRS 2 and HH 193 at PA$\sim$147°. The northern edge of the redshifted emission may be connected to the redshifted gas associated with the L1448N/L1448C sources via a faint bridge of emission. (5) There is redshifted emission that peaks on HH 277, which appears to be oriented nearly perpendicular to the long axis of our map. (6) There is blueshifted CO emission associated with the HH 267 knots, which lie at the northwestern edge of our map.

Figure 2 shows CO (thin lines) and isotopic ^{13}CO (thick lines) J=1$\rightarrow$0 spectra obtained in single-pointing observations toward four positions. The spectra shown in Figure 2(b), (c), & (d) were obtained at positions of strong outflow emission within our map boundary, and (a) was obtained just off the northwest corner of our map, near the HH 267 knots. The spectra in Figure 2(a) show a separate velocity feature at 0 km s^{-1} in both the CO and ^{13}CO spectra. It is interesting to note that this velocity feature corresponds to the V_{LSR} of three HH objects in this cloud: HH 196A, HH 196B, & HH 267B. The velocity integration limits used for the blue- and redshifted high-velocity gas shown in Figure 1(a) are indicated by the horizontal arrows. These integration limits were chosen conservatively, avoiding emission from the velocity feature at V_{LSR} =0 km s^{-1}.

3.2. Background: Individual Outflow Sources

3.2.1. The L1448C/L1448N Core

The CO outflow from L1448C has been studied extensively since its discovery, at which time it was recognized as a unique source due to its high collimation factor (approaching 10:1) and its extremely high velocities (± 70 km s^{-1} – Bachiller et al. 1990; Bachiller et al. 1995). Interferometric observations of the outflow, acquired with a $3'' \times 2.5''$ synthesized beam, were required to resolve the limb-brightened CO cavities at "low" velocities ($-12 \leq V_{LSR} \leq +16$ km s^{-1}) (Bachiller et al. 1995; Dutrey, Guilloteau, & Bachiller 1997). By modelling the interferometric CO channel maps, the outflow inclination angle was found to be $i = 70°$, implying actual jet velocities in excess of 200 km s^{-1}. The initial conical outflow opening half-angle was found to be $\phi/2 = 22.5°$ (Bachiller et al. 1995). The outflow cavity walls become parallel, however, $\approx 1'$ (= 0.08 pc) downstream from the driving source, with a width of $\sim 20''$. Therefore, in our OTF map, the L1448C outflow remains unresolved along its width.

The redshifted lobe of the L1448C outflow is deflected by $\sim 20°$ from its initial direction, from an initial position angle of $+160°$ to a final position angle of $+180°$ (Dutrey, Guilloteau, & Bachiller 1997). This change in direction of the redshifted flow axis occurs abruptly near the position of the CO "bullet" known as R3 (Bachiller et al. 1990; Dutrey, Guilloteau, & Bachiller 1997). A string of H_2 emission knots along PA= 180° extends for nearly two arcminutes, beginning about an arcminute southeast of L1448C (Eislöffel 2000).

Similarly, the blueshifted CO outflow lobe powered by L1448C starts out at a position angle of – 21° (Bachiller et al. 1995) or, equivalently, along P.A. = +159° , before being deflected through a total angle of $\sim$ 32° by the time it arrives an arcminute downstream (Davis & Smith 1995; Eislöffel 2000). This deflection is due to the collision of the blueshifted gas driven by L1448C with the redshifted outflow lobe powered by L1448N(A). The strongly radiative shock emission at the interaction region of these colliding flows is evident through various tracers: enhanced CO millimeter line emission at the site of the CO bullet "B3" of Bachiller et al. (1990), a far-infrared continuum emission peak (Barsony et al. 1998), high-excitation, shocked molecular hydrogen emission (Davis et al. 1994; Davis & Smith 1995), and the optically visible shock-excited gas of HH 197 (Bally et al. 1997). Barsony et al. (1998) have argued that the interaction of the blueshifted flow driven by L1448C with ambient dense gas may have triggered the formation of the L1448N protobinary.

Extrapolating from the vicinity of HH 197 along P.A. $\sim$ 127°, which is the axis of the blueshifted L1448C CO outflow after its deflection near HH 197 through knots I, R, and S (Davis & Smith 1995; Eislöffel 2000), leads directly to HH 267 (see also Figures 6 & 7). The measured radial velocities of the HH 267 knots (HH 267A: $V_{LSR} = -50$ km s^{-1}; HH 267B: $V_{LSR} = 0$ km s^{-1}; HH 267C: $V_{LSR} = -63$ km s^{-1} – Bally et al. 1997) and the velocity extent of the blueshifted CO observed by Bachiller et al. (1990) agree well. The reported terminal velocity for the L1448C flow is 70 km s^{-1} (Bachiller et al. 1990, 1995). These two facts led to the suggestion that HH 267 may be powered by L1448C (Barsony et al. 1998).

L1448N(A) and L1448N(B) form a close (7″ separation) protobinary (Terebey & Padgett 1997), which is unresolved in our OTF map. The redshifted portion of the L1448N(A) flow was first detected via its associated low-excitation molecular hydrogen emission (Davis & Smith 1995). Its exciting source was first correctly identified by Barsony et al. (1998). The corresponding blushifted lobe has been detected only in an extended, conical reflection nebulosity whose peak is estimated to lie 1.″5 west and 6″ north of L1448N(A) (Bally et al. 1993). The position angle of $\sim 150°$ for this flow is determined by the symmetry axis of the U-shaped shocked molecular hydrogen emission (Barsony et al. 1998; see also Eislöffel 2000) and from the axis of the highly-collimated redshifted CO jet driven by L1448N(A) as seen in the $V_{LSR} = +8$ km s^{-1} outflow channel map of Bachiller et al. (1995). Redshifted gas associated with the L1448N(B) flow first appears in the paper reporting the discovery of the L1448C outflow (Bachiller et al. 1990). The corresponding blueshifted outflow lobe from L1448N(B) was partially mapped by Bontemps et al. (1996). Barsony et al. (1998) noted that HH 196, a series of blueshifted optical emission knots (HH 196A: $V_{LSR} = 0$ km s^{-1}; HH 196B: $V_{LSR} = 0$ km s^{-1}; HH 196C: $V_{LSR} = -35$ km s^{-1}; HH 196D: $V_{LSR} = -37$ km s^{-1} – Bally et al. 1997) lie along the L1448N(B) outflow axis. The position angle of the L1448N(B) outflow is PA$\sim$129°. About 20″ northwest of L1448N(A) lies L1448NW. Recent observations suggest that L1448NW drives a small-scale H_2 outflow along an east-west direction (Eislöffel 2000). Although we do not detect a CO outflow associated with L1448NW with our spatial resolution, unpublished interferometric observations do indicate the presence of an E-W flow centered on L1448NW (Terebey 1998).

3.2.2. The L1448 IRS 2 Core

L1448 IRS 2 was confirmed as a Class 0 protostar by O'Linger et al. (1999), who reported a CO outflow associated with this source. The outflow's symmetry axis (PA$\sim$133°) and full opening angle ($\phi \sim 27°$) were inferred from (1) the location of HH 195A–D along this PA, (2) a fan-shaped reflection nebulosity with this opening angle which is seen in K′ emission (Hodapp 1994), (3) the positioning of CO "bullets" of emission at the 3σ level, along the outflow PA about 10′ to the northwest of IRS 2, and (4) the apparent V-shaped morphology of the blueshifted CO emission. This symmetry axis and initial opening angle are also evident in a recent H_2 2.12 μm image of L1448 (Eislöffel 2000; see also Figure 7).

3.3. Velocity Maps

In order to elucidate the velocity structure of the CO emission, Figures 4 & 5 present contoured greyscale maps of the integrated CO intensities for several velocity intervals blueward and redward, respectively, of the approximate ambient cloud velocity. Figure 3 labels the positions of all of the Herbig-Haro objects within our map boundary, as well as the Class 0 protostars and Class I source, IRS 1, and should be used to facilitate viewing Figures 4 & 5. For Figures 4 & 5, the highest velocity emission with respect to the ambient cloud (4a & 5a) have been integrated over 4 km s^{-1} intervals in order to obtain good signal-to-noise, and the subsequent maps have been integrated over 2 km s^{-1} intervals. The top 3 maps in each figure represent high-, intermediate-, and low-velocity gas for the

blueshifted (Figure 4) and redshifted (Figure 5) emission. The bottom 2 maps in each panel represent emission at velocities within the line core. The maps have been rotated so that the major axis of each map (PA=135° measured east from north) lies along a horizontal direction.

These maps shed more light on some of the outstanding features described in §3.1, and uncover additional interesting features that are not as apparent in the total integrated intensity outflow map of Figure 1a. It is immediately apparent from these maps that much of the emission within the line core delineates gas that has been entrained in the outflows. In particular, the $\sim$ 15′ long blueshifted feature is seen to some degree in all of the maps depicting emission blueward of the ambient cloud velocity (Figures 4a–e), as well as in the core gas redward of the ambient cloud velocity (Figures 5d & e). Redshifted, as well as blueshifted, CO emission surrounds HH 193. This is not surprising, since the radial velocities and linewidths of HH 193A, B, and C, are -18 & 40 km s^{-1}, 10 & 70 km s^{-1}, and -10 & 50 km s^{-1}, respectively (Bally et al. 1997). This significant overlap of blueshifted and redshifted emission strongly suggests that the blueshifted feature is oriented close to the plane of the sky.

At the highest velocities (Figures 4a & 5a), there is highly-collimated blue- and redshifted emission along PA$\sim$ 147°, centered on L1448 IRS 2. The blueshifted emission is part of the aforementioned $\sim$ 15′ long feature. It passes through HH 195A–D (but not HH 195E), and appears to culminate in HH 193, however it intersects a second blueshifted

feature eminating from the L1448N/L1448C region along P.A. $\sim$ 129° (figure 4a). The intersection occurs a couple of arcminutes downstream of the HH 196 knots. Another blueshifted feature branches off to the southwest a few arcminutes downstream from the HH 196 knots (Figure 4b). The redshifted emission along PA$\sim$ 147° from IRS 2 extends $\sim 9'$ southeast of IRS 2 (Figures 5a–c), where it shows a prominent peak in Figure 5b, as well as in the CO total integrated intensity outflow map in Figure 1a.

The blue- and redshifted peaks adjacent to L1448 IRS 2 are most prominent in the lowest-velocity outflow emission (Figures 4c & 5c). The blueshifted peak is spatially coincident with HH 195E. At higher velocities (Figures 4a & b), the blueshifted emission extends along a P.A.$\sim$120° from IRS 2, past IRS 1, and may continue past HH 194, which shows a local peak in blueshifted emission (Figures 4b & c). Curiously, the HH 194 knots are all *redshifted*, with very large linewidths (HH 194A: V_{LSR} =66 km s^{-1}, ΔV=110 km s^{-1}; HH 194B: V_{LSR} =66 km s^{-1}, ΔV=150 km s^{-1}; HH 194C: V_{LSR} =110 km s^{-1}, ΔV=60 km s^{-1}). HH 194C has been associated with redshifted outflow emission from IRS 1 (Bally et al. 1997). Although there is a prominent local peak in the blueshifted CO emission at the position of HH 194, there is no evidence of redshifted CO emission (figures 5a–c) at this position.

The extended redshifted emission directly to the southeast of L1448N/L1448C is also clearly present at core velocities, very strongly so in Figure 5d, and even in Figure 4e. The previously suggested structure along three separate axes is also seen in Figures 5a–c; mostly

strikingly, in Figure 5b. These three axes, along P.A. $\sim$ 180°, 150°, & 129°, correspond to the PAs of the redshifted lobes of the outflows associated with L1448C, L1448N(A), & L1448N(B), respectively. The redshifted feature that peaks on HH 277 is most prominent as a separate velocity feature in Figure 5c.

In the following section, we consider these features in connection with what is known about the individual outflows in order to interpret the outflow morphology in L1448.

3.4. Interpretation of Outflow Structure

Figure 6 indicates the various outflow position angles, superimposed on our integrated high-velocity CO map of Figure 1a, and based upon all of the available data. Colored solid lines are used to denote the extents of various outflow lobes that are well-established from the literature and our CO data. Colored dashed lines are used to indicate extrapolations that are less well-established, but reasonable models that are consistent with our data. Black dotted lines indicate the initial opening angle of the L1448 IRS 2 outflow. Our rather low, $\sim 1'$, resolution data were not used to define any of the flow axes, since in each case arcsecond-scale data are available from the published literature to define these axes. Figure 7 shows the various outflow position angles superimposed on a recent H_2 map of L1448 (Eislöffel 2000). (Please note that Figure 7 is the only figure we present in J2000 coordinates.) For all of the outflows, we find reasonably good agreement between large-scale CO features and flow axes that have been determined from higher-resolution observations.

The extents and directions of the L1448C outflow lobes, as inferred from prior observations, as well as from our CO data, are indicated by the solid green lines in Figure 6. The dashed green line on the blueshifted side represents the continuation of the blueshifted emission from L1448C proposed by Barsony et al. (1998), based on the final deflection angle of the blueshifted outflow and the similarities in the outflow velocity extent and observed velocities of the HH 267 knots. The blueshifted CO along PA$\sim$ 127°, associated with this extension of the L1448C flow, is clearly seen in Figures 1a & 6, and lies will to the south and west of the L1448N sources. Figure 7 indicates the blueshifted L1448C outflow axis passes directly through emission knots I & S, and about 20″ north of emission knot R. Emission knot R lies within more extended H_2 emission that appears to form a U-shaped or bow-shock structure which opens toward the southeast, bisecting the L1448C outflow axis. The sides of the U are separated by $\sim$ 40″, with the brighter side (including knot R) lying to the south of the L1448C outflow axis. The dashed green line on the redshifted side in Figure 6 indicates the possible continuation of the L1448C outflow to the south, whose presence is suggested by the bridge of redshifted CO emission that continues along this direction.

Only redshifted molecular gas associated with the L1448N(A) outflow, along PA$\sim$150°, is detected in our CO maps, with a total length of at least 0.7 pc. The U-shaped molecular hydrogen emission that traces part of the redshifted outflow cavity wall is unresolved in our CO maps. Knots of H_2 emission which trace the outflow wall are $\leq$30″ apart as far as 3′ to the southeast of L1448N(A) (Barsony et al. 1998; Eislöffel 2000 – see also our Figure

7). Taken together with the observed length of the CO redshifted lobe, this suggests a collimation factor of at least 16:1. The opening half-angle of the L1448N(A) outflow was estimated to be $\phi/2 \approx 25°$, from the morpholgy of the near-infrared reflection nebulosity to the north of L1448N(A), associated with what would be the blueshifted outflow lobe (Bally et al. 1993). The blueshifted flow powered by L1448N(A) is not apparent in our CO maps, judging by the drop in the blueshifted, high-velocity CO contour levels along the symmetry axis of its NIR reflection nebula. The lack of blueshifted CO emission from the L1448N(A) outflow is most likely accounted for by the likelihood that the cloud boundary has been reached in this direction, and that the flow has broken out of the molecular cloud.

The position angle, PA$\sim$129° of the L1448N(B) outflow was determined by the orientation of the redshifted CO outflow driven by L1448N(B) in Figure 1(b) and noting that this CO flow symmetry axis intersects HH 196 (Barsony et al. 1998). The true spatial extent of the L1448N(B) CO outflow, however, is demonstrated here for the first time. On the scale of our map, the L1448N(B) outflow remains unresolved along its width. The optical emission knots of HH 196 are indicated by crosses in Figure 6, and are, indeed, found to lie right along the L1448N(B) CO outflow axis, confirming the identification of L1448N(B) as their exciting source. The direction of the L1448N(B) outflow downstream of the HH 196 knots is unclear. The outflow may bend, possibly due to interaction with the IRS 2 outflow (see §4.2.), and culminate in the HH 193 knots, approximately 8′ further downstream from HH 196. Alternately, we note that if the outflow continues along PA$\sim$ 129°, it could account for the bulge in the blueshifted emission a couple of arcminutes

due south of HH 193 (Figure 1a, Figure 4c, Figure 6), and might even be responsible for exciting the three northernmost HH 267 knots. The full extent of the redshifted lobe associated with L1448N(B) is also unclear. HH 277 appears to be associated with its own redshifted CO velocity feature, which is seen most prominently in Figure 5c, and may be driven by a source off the edge of our map. Using the most conservative length for the L1448N(B) outflow, the major axis taken from the HH 196 knots through the end of the redshifted lobe ($\sim$12′), the derived lower limit for the collimation factor is $\geq$12:1. Estimates of the initial opening angle and width of the L1448N(B) outflow await higher spatial resolution, interferometric imaging.

The most distant part of the 15′−long blueshifted filament evident in Figure 1a cannot be due to either L1448N(A) or L1448C. The PA of the L1448N(A) outflow, deduced from the reflection nebulosity's symmetry axis as seen in Bally et al. 1993, Davis et al. 1994, and Davis & Smith 1995, misses the blue-shifted filament of Figure 6 completely. Neither is the HH 193 complex along the PA of L1448C flow, after its bend in the vicinity of HH 197. Although the blueshifted CO of the deflected outflow powered by L1448C may continue nearly parallel to the blueshifted CO lobe of the flow powered by L1448N(B), the L1448C flow lies well to the south of the L1448N(B) flow. Therefore, the HH 193 complex must be either excited by the L1448N(B) flow, if it bends in the vicinity of HH 196, or by an outflow from IRS 2.

There are several puzzling aspects to the IRS 2 outflow that are not easily explained by

the observations. At first glance, there appears to be a very confined outflow whose lobes peak only $\sim 1'$ from IRS 2. The redshifted peak is well-aligned with a line drawn through IRS 2 and extended through HH 195A-D, the previously proposed axis at PA$\sim$133° for the IRS 2 outflow (O'Linger et al. 1999). However, the blue peak closest to IRS 2 is skewed at a somewhat shallower position angle closer to PA$\sim$120°. No H_2 emission (Figure 7), or CO emission (Figure 1a, Figures 5a–c, Figure 6), is seen on the opposite side of IRS 2 along PA$\sim$120°, which would be expected if there were an outflow along this direction. The blue peak is spatially coincident with HH 195E, the only HH 195 knot which is off the axis of the IRS 2 outflow. It has been argued that IRS 1 drives an east-west oriented outflow and is the most probable driving source of HH 195E (Bally et al. 1997; Eislöffel 2000). Although the presence of an E-W oriented outflow in this region is undisputed, it is possible that an as yet undiscovered source, other than IRS 1, may be the responsible agent. In any event, the positioning of the blue peak so close to IRS 2 may be coincidental, and due primarily to local heating associated with HH 195E, and overlapping outflows associated with blueshifted emission from IRS 2 and the primarily E-W flow in this vicinity. This picture is supported by the L1448 H_2 mosaic (Eislöffel 2000; Figure 7), which indicates an E-W axis for the H_2 emission in the vicinity of HH 195E.

In the model put forth by O'Linger et al. (1999) for the IRS 2 outflow, the symmetry axis PA$\sim$133° and full opening angle $\phi \sim 27°$ imply that the outflow cavity walls lie along PA$\sim$147° and PA$\sim$120°. If the IRS 2 outflow retains its initial opening angle out to large distances, this would explain various blue- and redshifted features at large distances from

IRS 2, notably the V-shaped morphology of the blueshifted gas and the presence of several CO "bullets" located along the proposed outflow axis, well beyond HH 195A–D. In a constant opening angle outflow scenario, HH 193 lies along one arm of this V, at PA$\sim$147°. The blueshifted gas along the other arm of the V (PA$\sim$120°) would be confused with emission from the E-W outflow in this vicinity, but since the blueshifted emission extends *past* IRS 1 towards the *redshifted* HH 194 knots, at least part of this emission may be due to IRS 2. Although there is redshifted CO emission along PA$\sim$133° and along PA$\sim$147°, there is little evidence for redshifted emission along PA$\sim$120°. However, this may be due to confusion with the three redshifted lobes associated with L1448C, L1448N(A), & L1448N(B).

Figure 7 clearly shows an outflow associated with IRS 2 along a PA$\sim$133°. The redshifted gas along the outflow axis is prominent in the H_2 emission, but not clearly apparent in our CO maps beyond the redshifted peak about 1′ southeast of IRS 2. Hints of more extended emission along PA$\sim$133° may be seen, however, in Figures 5b & c, and curiously, in *blueshifted* emission extended along this axis to the southeast of IRS 2 in Figure 4d. Such overlap of blueshifted gas along the redshifted outflow axis is expected for outflows oriented nearly in the plane of the sky. Indications of extended blueshifted emission along PA$\sim$ 133°, at least a few arcminutes downstream of HH 195A–D, are seen in Figures 4b & c.

There are a few problems with the constant opening angle model however. Figure 7

indicates that although the initial opening angle of the IRS 2 outflow is $\phi \sim 27°$, the two strands of H_2 defining this opening angle join in a bow shock structure in the vicinity of HH 195A-D. Also, we note that the highest-velocity outflow emission is expected to be confined to the outflow axis, but the highest-velocity CO gas we observe is along PA$\sim$147°, *not* along PA$\sim$133°. However, our maps are probably not sensitive enough to have picked up the highest-velocity outflow emission, which would in any case be severely diluted in our large ($\sim$1′) beam.

An alternate scenario which could explain the morphology of the high-velocity CO emission associated with IRS 2 would be to postulate *two* outflows from IRS 2, the confirmed outflow along PA$\sim$133°, and another outflow along PA$\sim$147°. In this scenario, IRS 2 would be the most likely exciting source of HH 193. If there is a second outflow along PA$\sim$147°, it is only detected in the CO emission, not the H_2 emission. Two outflows, along distinctly different position angles would also suggest that IRS 2 might be a binary system. However, there is no evidence to indicate this source to be a binary from any of the IRAS or SCUBA data (Barsony et al. 1998; O'Linger et al. 1999). This means that were IRS 2 a binary system, it would have to be binary on a scale smaller than 7 arcsec (the resolution limit at 450 microns of the JCMT SCUBA data). Only arcsec/sub-arcsec imaging at either millimeter or centimeter wavelengths could test the binary hypothesis further. Although it is possible that there is a second outflow along PA$\sim$147°, much of the blueshifted emission could be explained by a bend in the jet emanating from L1448N(B), possibly due to interaction with the IRS 2 CO outflow wall (see §4.2.).

Finally, although the origin of the HH 267 knots cannot definitively be resolved based on the CO data we present here, our observations do constrain the driving source. L1448N(A) can be ruled out as the possible driving source of HH 267, since the PA of its outflow is along a completely different direction than the line linking it with HH 267. Furthermore, blue-shifted molecular gas has yet to be detected from this source. L1448N(B) may be the exciting source of the northernmost HH 267 knots (HH 267A, B, & C) if it is not deflected, as suggested, downstream of HH 196, but the outflow axis completely misses the two southernmost HH 267 knots. This leaves either the L1448 IRS 2 blueshifted flow or the deflected blueshifted L1448C flow as the most plausible exciting sources, at least for HH 267D & HH 267E. The PA of the IRS 2 outflow axis, as deduced in O'Linger et al. (1999), and Figure 7, misses the HH 267 complex. However, the PA of the deflected blueshifted lobe of the L1448C flow goes right through HH 267D & HH 267E.

If HH 267 is powered by L1448C, then the full extent of the blueshifted flow from L1448C would be 2.3 pc, with a collimation factor (length/width ratio) of $\sim$ 64:1. The full length of the deflected redshifted flow powered by L1448C is unclear, since it becomes confused with redshifted emission from IRS 2 a few arcminutes south of L1448C.

4. DISCUSSION

4.1. CO Outflow Re-Collimation

The CO outflows powered L1448C, L1448N(A), and L1448N(B), which all have nearly identical initial opening angles ($\phi/2 = 22.5°$, $\sim 25°$, and $\leq 25°$, respectively) are recollimated within 0.1 pc of their origins. Once re-collimated, these flows maintain their collimation (i.e., appear unresolved in our maps) along their respective lengths. This same structure is observed in the outflow from the prototypical Class 0 source, VLA 1623 (Dent, Matthews, & Walter 1995).

The L1448 IRS 2 outflow may be unique among the L1448 protostellar outflows in that it appears to retain its initial opening angle ($\phi/2 = 13.5°$) over a greater distance than the other outflows, possibly over parsec length scales. A large-scale, biconical outflow morphology would account for the presence of both blue- and redshifted high velocity gas observed in regions which are not intersected by the highly collimated outflows from L1448C, L1448N(A), or L1448N(B). We note that L1448 IRS 2 is located in its own NH_3 core ($V_{LSR} = 4.2$ km s^{-1}), distinct from the NH_3 core ($V_{LSR} = 4.7$ km s^{-1}) containing the sources L1448C, L1448N(A), and L1448N(B) (Bachiller et al. 1986a).

4.2. Colliding Molecular Outflows in L1448?

Viewing the three-dimensional problem of the probability of collisions among highly-collimated outflows, one might, in general, expect a rather small probability of collisions. However, for the case of the L1448 outflows, it is clear that they all have high inclination angles to the line-of-sight ($\geq 70°$). Limits may be placed on the inclination angle of the L1448 IRS 2 outflow by noting the presence of overlapping blue- and redshifted emission in the outflow. For a constant opening angle of $\phi = 27°$, the inclination angle must be i>63° for such overlap to occur. The individual outflow position angles are well-determined. Therefore, if we assume that the outflows which are unresolved along their minor axes in our beam (L1448C, L1448N(A), & L1448N(B)) are "pencil-thin" (outflow walls nearly parallel) at larger distances from their driving sources, and that these outflows maintain their "final" position angles (discussed in §3) over large distances, then outflow collisions with the L1448 IRS 2 outflow are expected to occur if the relative difference between the inclination of either the L1448C, L1448N(A), or L1448N(B) outflows and the L1448 IRS 2 outflow is $\leq 13.5°$ (the half-opening angle of the L1448 IRS 2 outflow).

The L1448N(B) axis and proposed IRS 2 outflow wall intersect in the plane of the sky a little more than an arcminute downstream of HH 196. The L1448N(B) outflow may be redirected to a steeper position angle here, to excite HH 193. The only other known candidate for exciting HH 193 is IRS 2 itself, either along the outflow wall, or by a second outflow emanating from IRS 2, along PA$\sim$ 147°.

4.3. Cloud Dispersal by Giant Protostellar Flows?

The most dramatic evidence for the direct effects of the outflows on the L1448 molecular cloud is seen in the distortions of the cloud contours at all velocities in Figures 4 & 5. It is difficult to understand how the "pencil-thin" outflows eminating from the L1448C/L1448N core could have such a dramatic effect on the morphology of the entire cloud. One possibility is that the L1448 cloud is highly prolate in shape, with its long axis in the plane of the sky.

Although we cannot estimate the masses and energetics of each individual outflow in our maps due to confusion in space and velocity, we can, nevertheless, estimate the *total* contribution of the outflows to the cloud's energetics. The Local Thermodynamic Equilibrium (LTE) analysis used to estimate the combined mass of the outflows ($M_{tot} \approx 0.7$ $M_{\odot}$) is discussed in O'Linger et al. (1999). Optically thin high-velocity CO emission was assumed, given the lack of observed high-velocity ^{13}CO emission in the velocity intervals outside the cloud core (see Figure 2). Therefore, the resultant derived mass is a strict lower limit, since no attempt was made to correct for the considerable mass expected to be masked by the line core emission.

For highly inclined outflows ($i > 70°$), the characteristic velocity which is used to calculate outflow energetic parameters is best chosen as the geometrical mean between the highest observed velocities, V_{CO}, and the inclination-corrected velocity, $V_{CO}/cos(i - \frac{\phi}{2})$, where $\frac{\phi}{2}$ is the half-opening angle of the outflow (Cabrit & Bertout 1992). Assuming the

outflow inclinations, $70° \leq i \leq 90°$, $V_{char} = 22 - 34$ km s^{-1} for the L1448 outflows, the total momentum contained in the four protostellar flows is computed to be 16 $M_\odot$ km s^{-1} $\leq M_{tot}V_{char} \leq 24$ $M_\odot$ km s^{-1}. This range of values is nearly equivalent to the momentum content of the quiescent NH_3 cores, assuming 50 $M_\odot$ total cores and $v_{turb} \sim 0.5$ km s^{-1} (Bachiller & Cernicharo 1986a). Even more striking, the total kinetic energy of the four protostellar flows, 2×10^{45} ergs $\leq \frac{1}{2}M_{tot}V_{char}^2 \leq 8\times10^{45}$ ergs, exceeds the gravitational binding energy ($\sim\ GM^2/R\ \approx 5 \times 10^{44}$ ergs) of the NH_3 cores by an order of magnitude, and the gravitational binding energy of the 100 $M_\odot$ $C^{18}O$ cloud (9×10^{44} ergs), contained within a 1.3 pc $\times$ 0.7 pc region (Bachiller & Cernicharo 1986b), by a factor of five.

The total outflow momentum quoted above is, in fact, a lower limit, since these outflows are still gaining momentum from the force provided by the central driving engines, and the total outflow mass may be grossly underestimated. The magnitude of both the total energy and momenta of the outflows suggests these outflows are capable of dispersing the NH_3 cores.

5. Summary

• Spectral-line "on-the-fly" mapping was used at the NRAO 12-meter millimeter telescope to produce a large-scale ($47' \times 7'$) CO (J=1→0) map of the L1448 dark cloud, sensitive enough ($1\ \sigma = 0.1$K) to enable the detection of outflow activity on parsec-scales and the identification of at least four distinct, protostellar molecular outflows. Large-scale,

high-spatial resolution optical and near-infrared images of shocked gas emission regions associated with each outflow were crucial for identifying the CO counterparts of the four protostellar flows.

• We confirm the deflection of the L1448 C outflow just south of L1448N(A) & (B), and present suggestive evidence of deflection of the L1448N(B) blueshifted jet by interaction with an outflow from IRS 2.

• The L1448 IRS 2 outflow may be unique in maintaining its initial opening angle, $\phi/2 = 13.5°$, out to large, possibly parsec-scale, distances. The other three parsec-scale protostellar flows in L1448 are re-collimated ≈ 0.1 pc downstream from their respective sources, with their outflow walls becoming parallel, and remaining so. In this context, we note that L1448 IRS 2 is forming in an NH_3 core which is distinct from the one containing the other three protostars. In an alternate scenario, there may be two distinct outflows emanating from an as yet unresolved binary system within L1448 IRS 2.

• The ambient cloud emission contours are severely disturbed by the outflows, suggesting a large fraction of the ambient cloud in the mapped region has been entrained in, or stirred up by, the outflows.

• The total outflow kinetic energy ($> 2 \times 10^{45}$ ergs) and combined outflow momenta (> 16 $M_\odot$ km s^{-1}) indicate that the outflows are energetically, and probably dynamically, capable of dispersing the 1 pc $\times$ 0.5 pc area, 50 $M_\odot$ total NH_3 cores in which the protostellar driving sources of the four outflows, L1448C, L1448N(A), L1448N(B), and L1448 IRS 2, are

currently forming, with the caveat that it is unclear, from both the outflow and ambient cloud morphology, whether the outflow momenta can be adequately transferred to the surrounding core.

ACKNOWLEDGEMENTS: We thank Dr. Darrel Emerson, Dr. Eric Greisen, and Dr. Jeff Mangum of NRAO for the development, implementation, and improvement of the spectral-line On-The-Fly mapping capability of the 12-meter telescope. GWC, JO, and MB gratefully acknowledge financial support from NSF grant AST-0096087 while part of this work was carried out. Part of this work was performed while GWC held a President's Fellowship from the University of California. MB's NSF POWRE Visiting Professorship at Harvey Mudd College, NSF AST-9731797, provided the necessary time to bring this work to completion. JO acknowledges financial support by the NASA Grant to the Wide-Field Infrared Explorer Project at the Jet Propulsion Laboratory, California Institute of Technology.

REFERENCES

Anglada, G., Rodríguez, L. F., Torrelles, J. M., Estalella, R., Ho, P. T. P., Cantó, J., López, R., & Verdes-Montenegro, L. 1989, ApJ, 31, 208

Bachiller, R. & Cernicharo, J. 1986a, A&A, 168, 262

Bachiller, R. & Cernicharo, J. 1986b, A&A, 166, 283

Bachiller, R., Cernicharo, J., Martin-Pintado, J., Tafalla, M., & Lazareff, B. 1990, A&A, 231, 174

Bachiller, R., Terebey, S., Jarrett, T., Martin-Pintado, J., Beichman, C.A., & Van Buren, D. 1994, ApJ, 437, 296

Bachiller, R., Guilloteau, S., Dutrey, A., Planesas, P., & Martin-Pintado, J., 1995, A&A, 299, 857

Bally, J., Lada, E.A., & Lane, A.P. 1993, ApJ, 418, 322

Bally, J., Devine, D., & Reipurth, B. 1996a, ApJ, 473, L49

Bally, J., Devine, D., & Alten, V. 1996b, ApJ, 473, 921

Bally, J., Devine, D., & Alten, V., & Sutherland, R.S. 1997, ApJ, 478, 603

Bally, J., Reipurth, B., Lada, C.J., & Billawala, Y. 1999, AJ, 117, 410

Barsony, M., Ward-Thompson, D., André, P., & O'Linger, J. 1998, ApJ, 509, 733

Bence, S.J., Richer, J.S., & Padman, R. 1996, MNRAS, 279, 866

Bence, S.J., Padman, R., Isaak, K.G., Wiedner, M.C., & G.S. Wright 1998, MNRAS, 299, 965

Bertoldi, F. & McKee, C.F. 1996 in Amazing Light: A Volume Dedicated to C.H. Townes on his 80th Birthday, ed. R.Y. Chiao, New York:Springer

Bontemps, S., Andr'e, P., Terebey, S., & Cabrit, S. 1996, A&A, 311, 858

Cabrit, S. & Bertout, C. 1992, A&A, 261, 274

Curiel, S., Raymond, J. C., Rodríguez, L. F., Cantó, J. & Moran, J. M. 1990, ApJ, 365, L85

Davis, C. J., Dent, W. R. F., Matthews, H. E., Aspin, C., & Lightfoot, J. F. 1994, MNRAS, 266, 933

Davis, C. J., & Smith, M. D. 1995, ApJ, 443, L41

Dent, W.R.F., Matthews, H.E., & Walther, D.M. 1995, MNRAS, 277, 193

Devine, D., Bally, J., Reipurth, B., & Heathcote, S. 1997, AJ, 114, 2095

Dutrey, A., Guilloteau, S., & Bachiller, S. 1997, A&A, 325, 758

Eislöffel, J. 2000, A&A, in press

Eislöffel, J. & R. Mundt 1997, AJ, 114, 280

Gomez, M., Whitney, B., & Kenyon, S.J. 1997, AJ, 114, 1138

Gomez, M., Whitney, B., & Wood, K. 1998, AJ, 115, 2018

Guilloteau, S., Bachiller, R., Fuente, A., & Lucas, R. 1992, A&A, 265, L49

Hodapp, K.-W. 1994, ApJS, 94, 615

Lada, C.J. & Fich, M. 1996, ApJ, 459, 638

Norman, C. & Silk, J. 1979, ApJ, 234, 86

O'Linger, J., Wolf-Chase, G.A., Barsony, M., & Ward-Thompson, D. 1999, ApJ, 515, 698

Reipurth, B., Devine, D., & Bally, J. 1998, AJ, 116, 1396

Sandell, G., & Knee, L.B.G. 1998, J. R. Astron. Soc. Ca., 92, 32

Terebey, S. 1998, private communication

Terebey, S. & Padgett, D. 1997, in IAU Symposium 182, Herbig-Haro Flows and the Birth of Low-Mass Stars, eds. B. Reipurth & C. Bertout (Dordrecht: Kluwer)

White, G.J., Casali, M.M., & Eiroa, C. 1995, A&A, 298, 594

Wilking, B.A., Schwartz, R.D., Fanetti, T.M., & Friel, E.D. 1997, PASP, 109, 549

This manuscript was prepared with the AAS LaTeX macros v4.0.

Fig. 1.— **High-velocity CO Outflow Emission on Large and Small Scales in the L1448 Dark Cloud**

a. Blue contours indicate high-velocity blueshifted ($-12.1 \leq V_{LSR} \leq -1$ km s^{-1}) emission and red contours indicate high-velocity redshifted ($+8.1 \leq V_{LSR} \leq +17.8$ km s^{-1}) CO J=1→0 emission in the $47' \times 7'$ region we mapped with the NRAO 12-m telescope. Contour levels start at 2 K km s^{-1} ($\approx 3\ \sigma$), and increase in 1.5 K km s^{-1} intervals. For comparison, the dashed rectangle shows the approximate area previously mapped (in CO J=2→1), shown in the inset. Stars indicate the positions of Class 0 sources (L1448N refers to L1448N(A) & L1448N(B), which are unresolved by our beam), and the filled box indicates the position of the Class I source L1448 IRS 1. The 55″ FWHM NRAO beamsize is indicated in the lower right-hand corner. **b.** The previous CO J=2→1 IRAM 30-m map of high-velocity gas in L1448 (from Bachiller et al. 1990): Solid contours indicate high-velocity, blueshifted ($-$ 55 km s$^{-1} \leq V_{LSR} \leq 0$ km s^{-1}) gas, and dotted contours indicate high-velocity, redshifted ($+$ 10 km s$^{-1} \leq V_{LSR} \leq +$ 65 km s^{-1}) gas. First contour and contour intervals are at 10 K km s^{-1}. In addition to the famous protostellar outflow powered by L1448C, the weaker outflow, powered by L1448N(B), is also detected . The 12″ FWHM IRAM beamsize is indicated in the lower right-hand corner.

Fig. 2.— ^{12}CO (thin solid line) & ^{13}CO (thick solid line) J=1→0 spectra obtained at the four positions on our map whose B1950 coordinates are indicated: (a) CO spectra near the HH 267 knots (just off the northwest corner of our map) clearly show two separate

velocity components: a brighter component at the same velocity as HH 267B, V_{LSR} =0 km s^{-1} (thin vertical dashed line), and a dimmer component at V_{LSR} =4.25 km s^{-1} (thick vertical dashed line). (b) – (d) CO spectra show strong CO self-absorption at the ambient cloud velocity, V_{LSR} =4.25 km s^{-1}. Arrows indicate the velocity ranges used to determine integrated intensities, masses, and energetics for the outflow emission.

Fig. 3.— Template for figures 4 & 5, labelling the positions of all the Herbig-Haro objects (tilted black crosses), the Class I source IRS 1 (filled red box), and the Class 0 protostars IRS 2, L1448C, L1448N(A & B), and L1448NW (red stars). L1448N & NW are not resolved in our 55″ beam. The separation between L1448C & L1448N is $\sim$ 75″.

Fig. 4.— Contoured greyscale images of the integrated CO intensity over velocity intervals blueward of the ambient cloud emission. Velocity intervals, lowest contour levels, and contour intervals, are, respectively: (a) -8 to -4 km s^{-1}, 1 K km s^{-1}, 0.5 K km s^{-1}; (b) -4 to -2 km s^{-1}, 1 K km s^{-1}, 0.5 K km s^{-1}; (c) -2 to 0 km s^{-1}, 1.5 K km s^{-1}, 1 K km s^{-1}; (d) 0 to 2 km s^{-1}, 2 K km s^{-1}, 2 K km s^{-1}; and (e) 2 to 4 km s^{-1}, 2 K km s^{-1}, 2 K km s^{-1}. Positions of Herbig-Haro objects (tilted yellow crosses), IRS 1 (filled red box), and Class 0 objects (red stars) are indicated.

Fig. 5.— Contoured greyscale images of the integrated CO intensity over velocity intervals redward of the ambient cloud emission. Velocity intervals, lowest contour levels, and contour intervals, are, respectively: (a) 12 to 16 km s^{-1}, 1 K km s^{-1}, 1 K km s^{-1}; (b) 10 to 12 km s^{-1}, 1 K km s^{-1}, 1 K km s^{-1}; (c) 8 to 10 km s^{-1}, 2 K km s^{-1}, 1 K km s^{-1}; (d) 6 to 8 km

s^{-1}, 2 K km s^{-1}, 2 K km s^{-1}; and (e) 4 to 6 km s^{-1}, 2 K km s^{-1}, 2 K km s^{-1}. Positions of Herbig-Haro objects (tilted yellow crosses), IRS 1 (filled red box), and Class 0 objects (red stars) are indicated.

Fig. 6.— Individual outflow position angles and extents superimposed on the CO outflow integrated intensity map of Figure 1a. Positions of all the Herbig-Haro objects (black crosses) are shown, as well as the five Class 0 sources (black stars), of which four are driving identifiable CO outflows in our data, and the Class I source, IRS 1 (solid black box). Position angles are indicated for the outflows associated with L1448C (green), L1448N(B) (mustard), L1448N(A) (purple, only redshifted outflow gas detected), and IRS 2 (black). For IRS 2, the opening angle of the ouflow is also indicated (dotted black lines). The extents of the outflow lobes that are well-established from the literature and our data (solid lines), as well as extrapolations that are consistent with our data, are shown (dashed lines). For clarity, the axis of the IRS 2 flow has not been extended beyond the region traced by the H_2 emission (see also Figure 7). Two possible extensions of the L1448N(B) outflow are indicated (dashed mustard lines).

Fig. 7.— Individual outflow position angles superimposed on an H_2 mosaic of L1448 (Eislöffel 2000). Note that the axes of this figure are in J2000 coordinates. The positions of Herbig-Haro objects (orange crosses), Class 0 sources (red stars), and IRS 1 (open red box), are indicated. Position angles of outflows are indicated as in Figure 6. Note that after its bend at emission knot I, the position angle of the L1448C outflow passes directly through emission

knot S. Although emission knot R lies about 20″ south of the outflow axis, this knot appears to be part of extended emission that forms a U-shaped structure which opens toward the southeast, bisecting the outflow axis. The sides of the U are separated by $\sim$ 40″, with the brighter side (including knot R) lying to the south of the L1448C outflow axis.

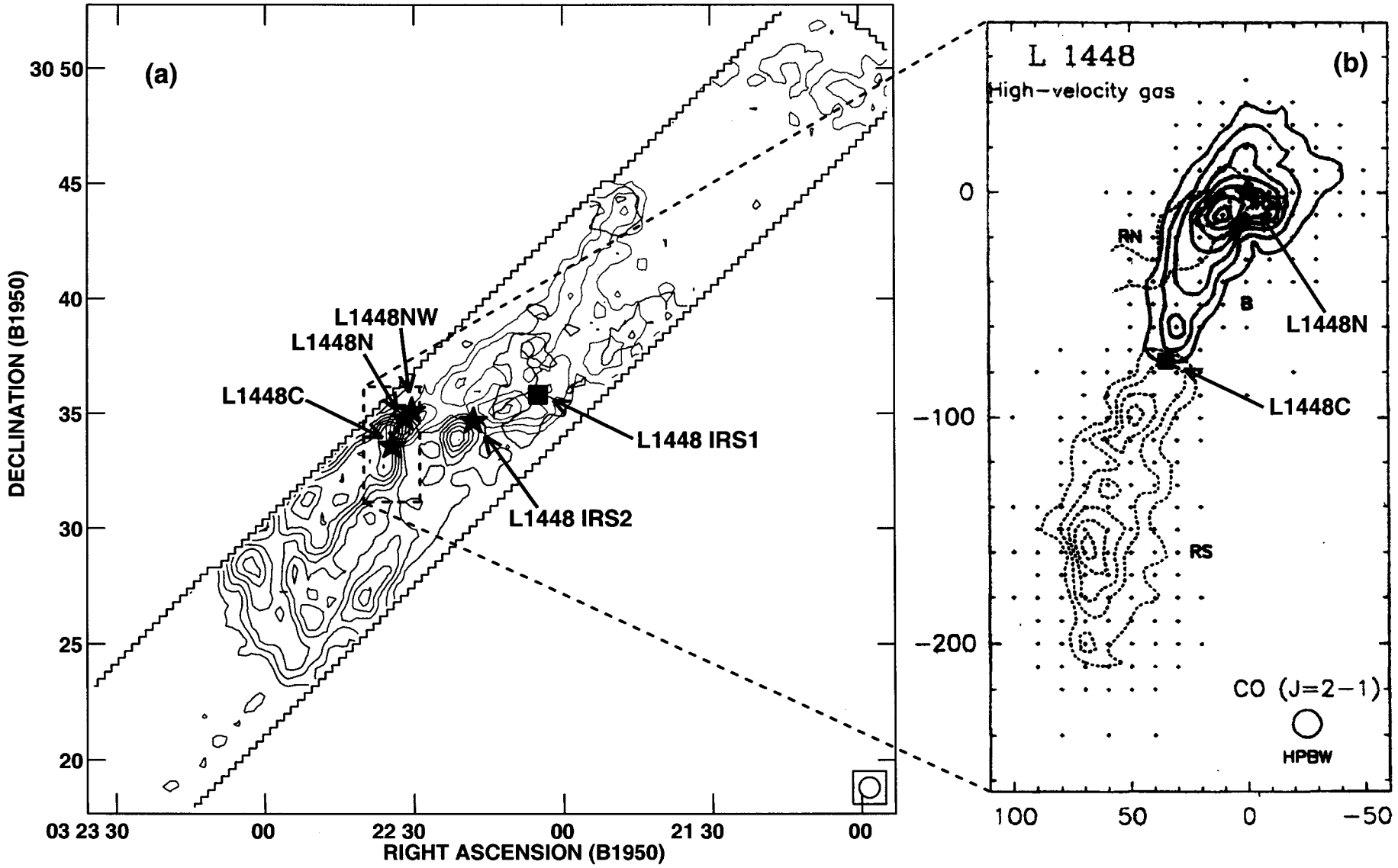
(a)
30 50
45
40
35
30
25
20
DECLINATION (B1950)
03 23 30
00
22 30
00
21 30
00
RIGHT ASCENSION (B1950)
L1448NW
L1448N
L1448C
L1448 IRS1
L1448 IRS2
L 1448
High−velocity gas
(b)
0
−100
−200
RN
B
L1448N
L1448C
RS
CO (J=2−1)
HPBW
100
50
0
−50

Fig 7

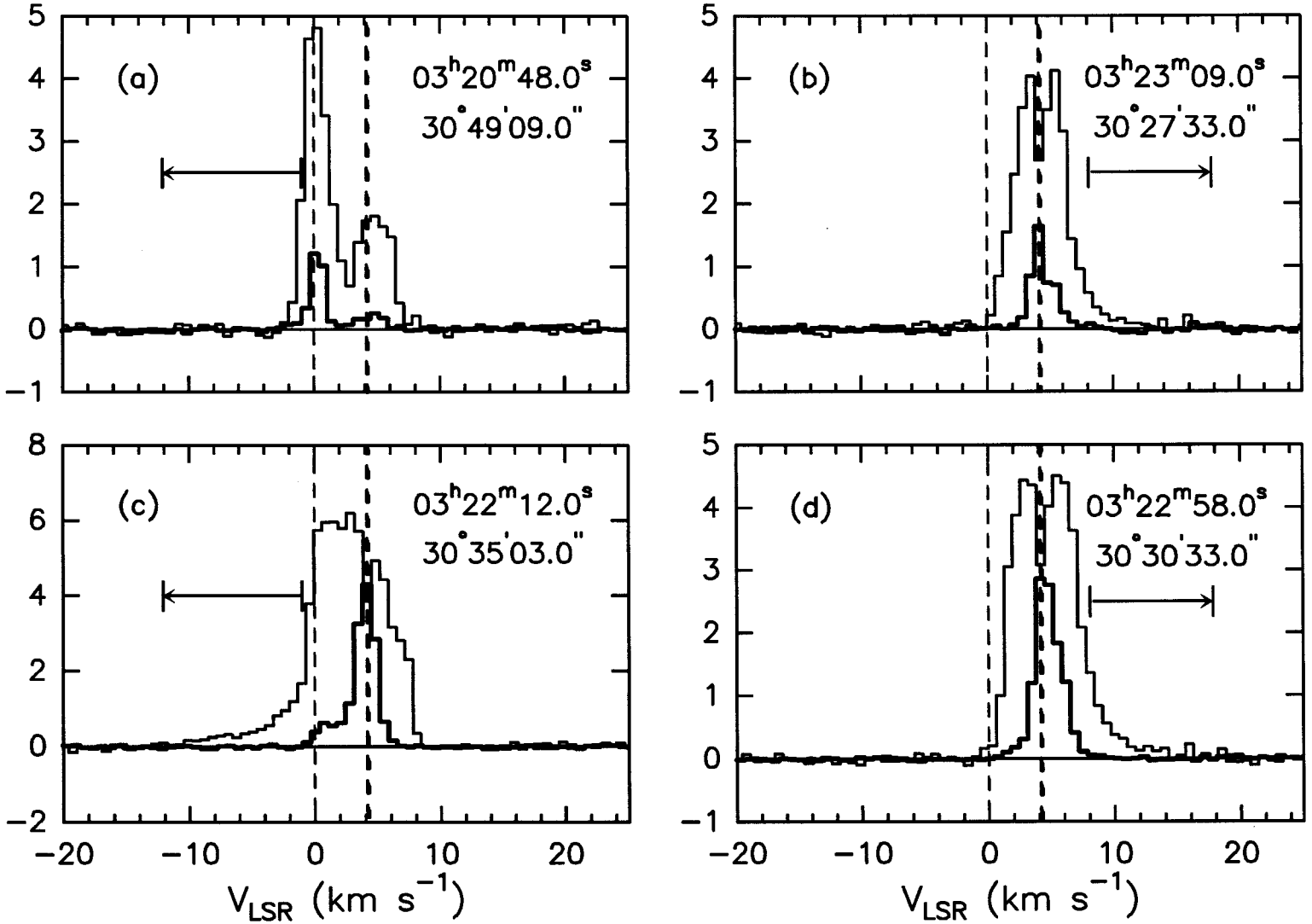
(a)
03h20m48.0s
30°49'09.0"
(b)
03h23m09.0s
30°27'33.0"
(c)
03h22m12.0s
30°35'03.0"
(d)
03h22m58.0s
30°30'33.0"
T*R (K)
T*R (K)
VLSR (km s−1)
VLSR (km s−1)

Fig 2

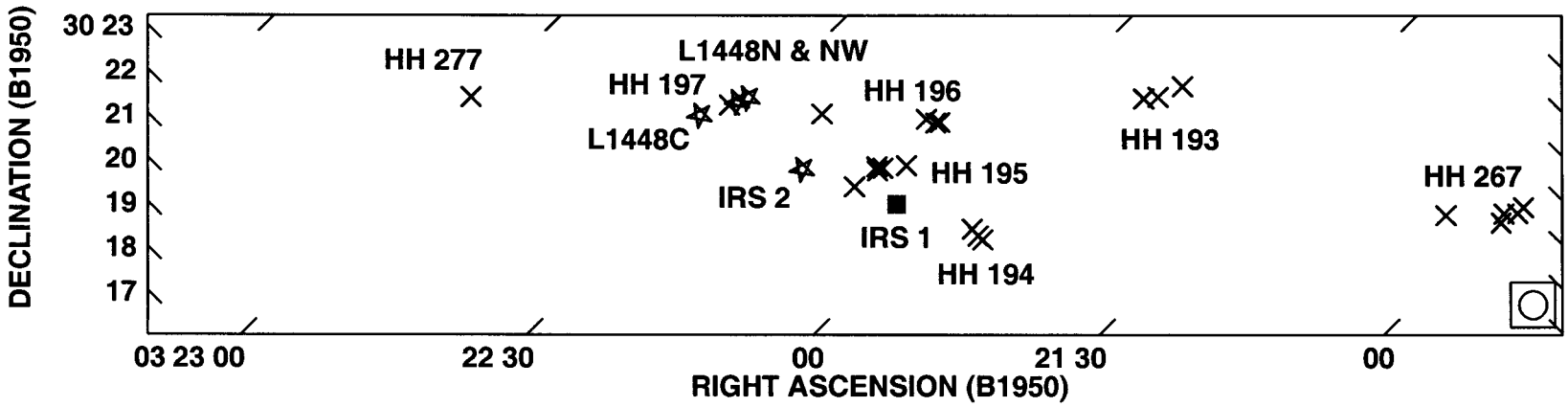
DECLINATION (B1950)
30 23
22
21
20
19
18
17
HH 277
L1448N & NW
HH 197
HH 196
L1448C
HH 193
HH 195
HH 267
IRS 2
IRS 1
HH 194
03 23 00
22 30
00
21 30
00
RIGHT ASCENSION (B1950)

Fig 3

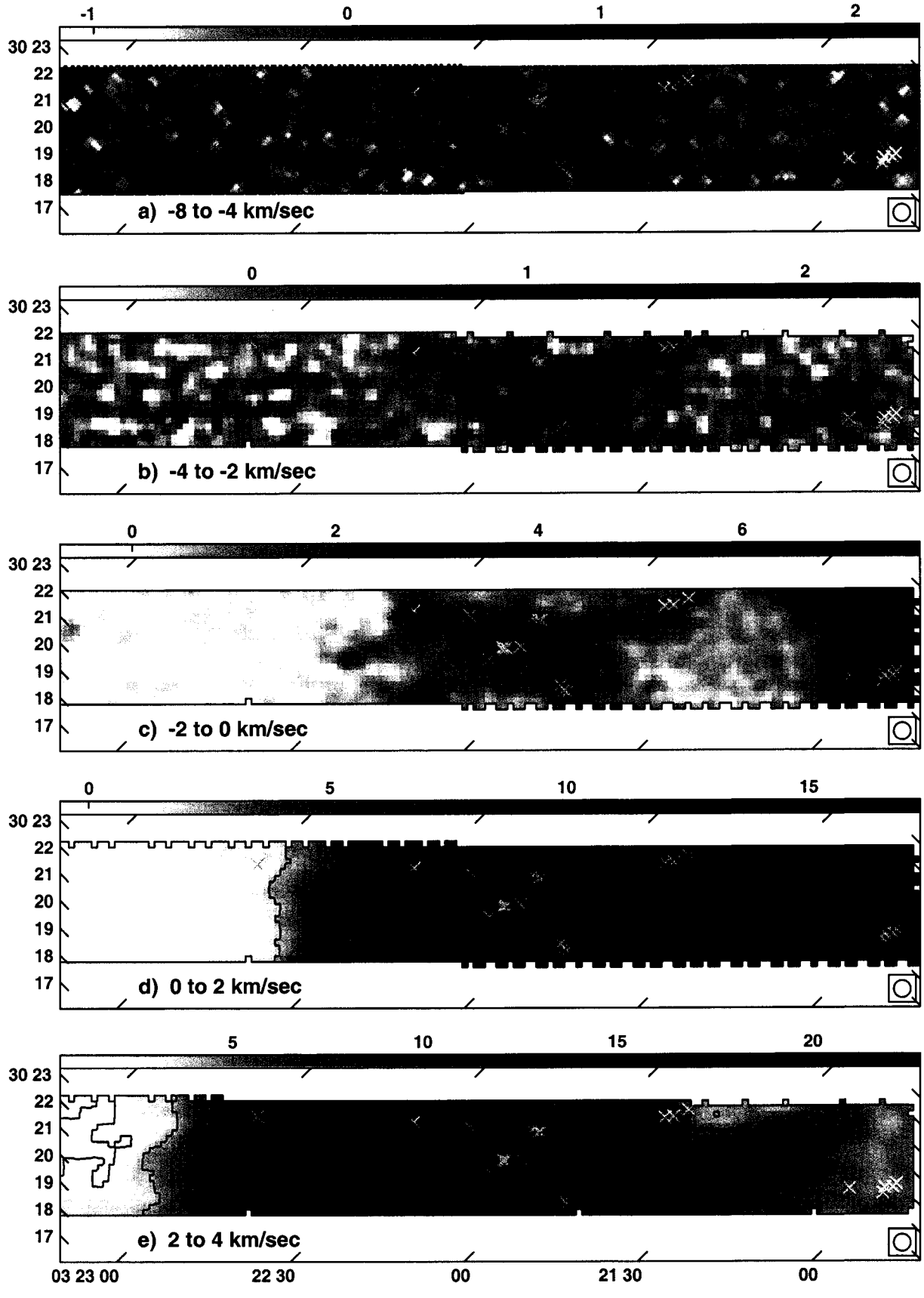
-1
0
1
2
30 23
22
21
20
19
18
17
a) -8 to -4 km/sec
0
1
2
b) -4 to -2 km/sec
0
2
4
6
c) -2 to 0 km/sec
0
5
10
15
d) 0 to 2 km/sec
5
10
15
20
e) 2 to 4 km/sec
03 23 00
22 30
00
21 30
00
DECLINATION (B1950)
RIGHT ASCENSION (B1950)

Fig 4

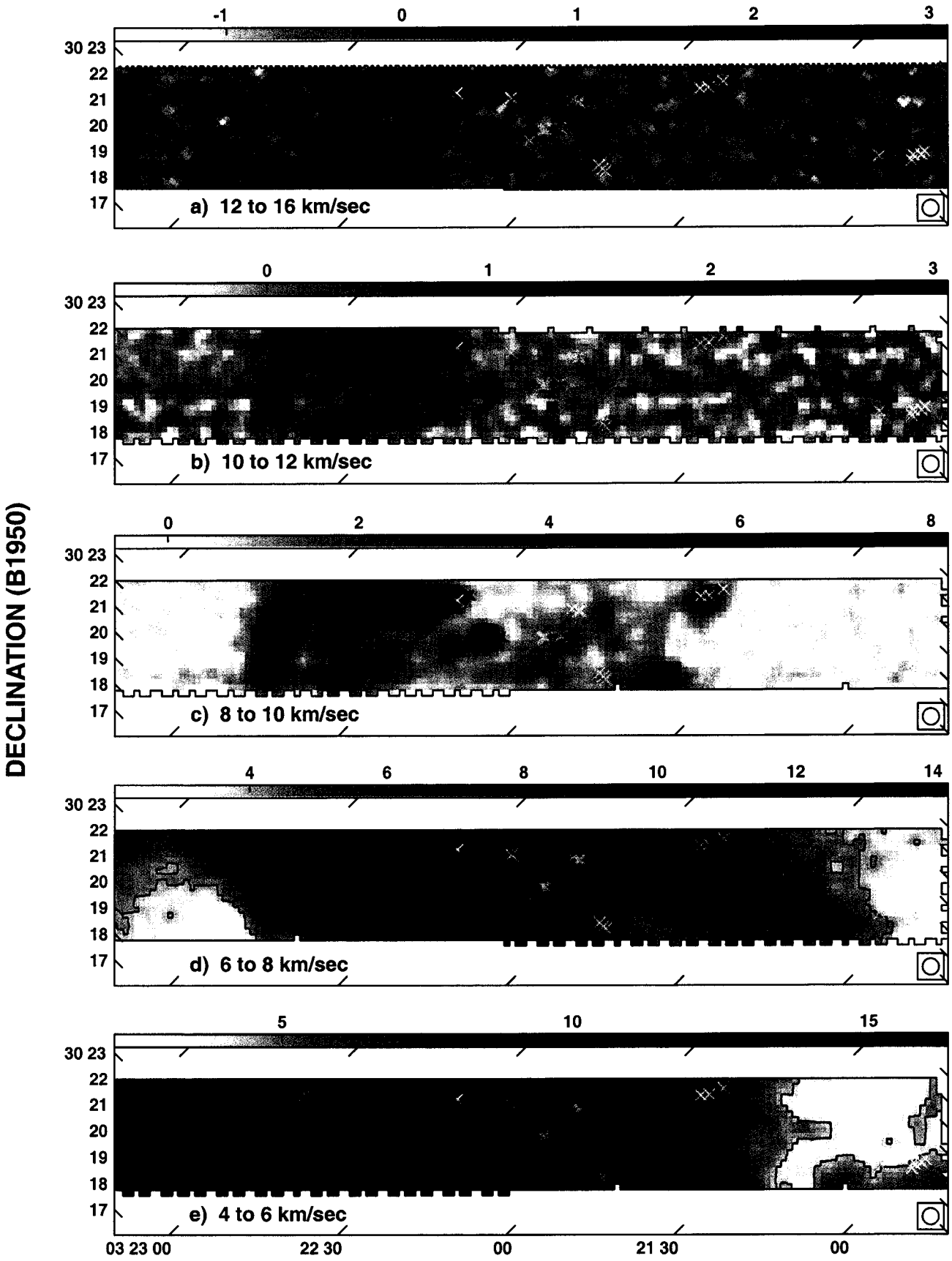
-1
0
1
2
3
30 23
22
21
20
19
18
17
a) 12 to 16 km/sec
0
1
2
3
b) 10 to 12 km/sec
0
2
4
6
8
c) 8 to 10 km/sec
4
6
8
10
12
14
d) 6 to 8 km/sec
5
10
15
e) 4 to 6 km/sec
03 23 00
22 30
00
21 30
00
DECLINATION (B1950)
RIGHT ASCENSION (B1950)

Fig 5

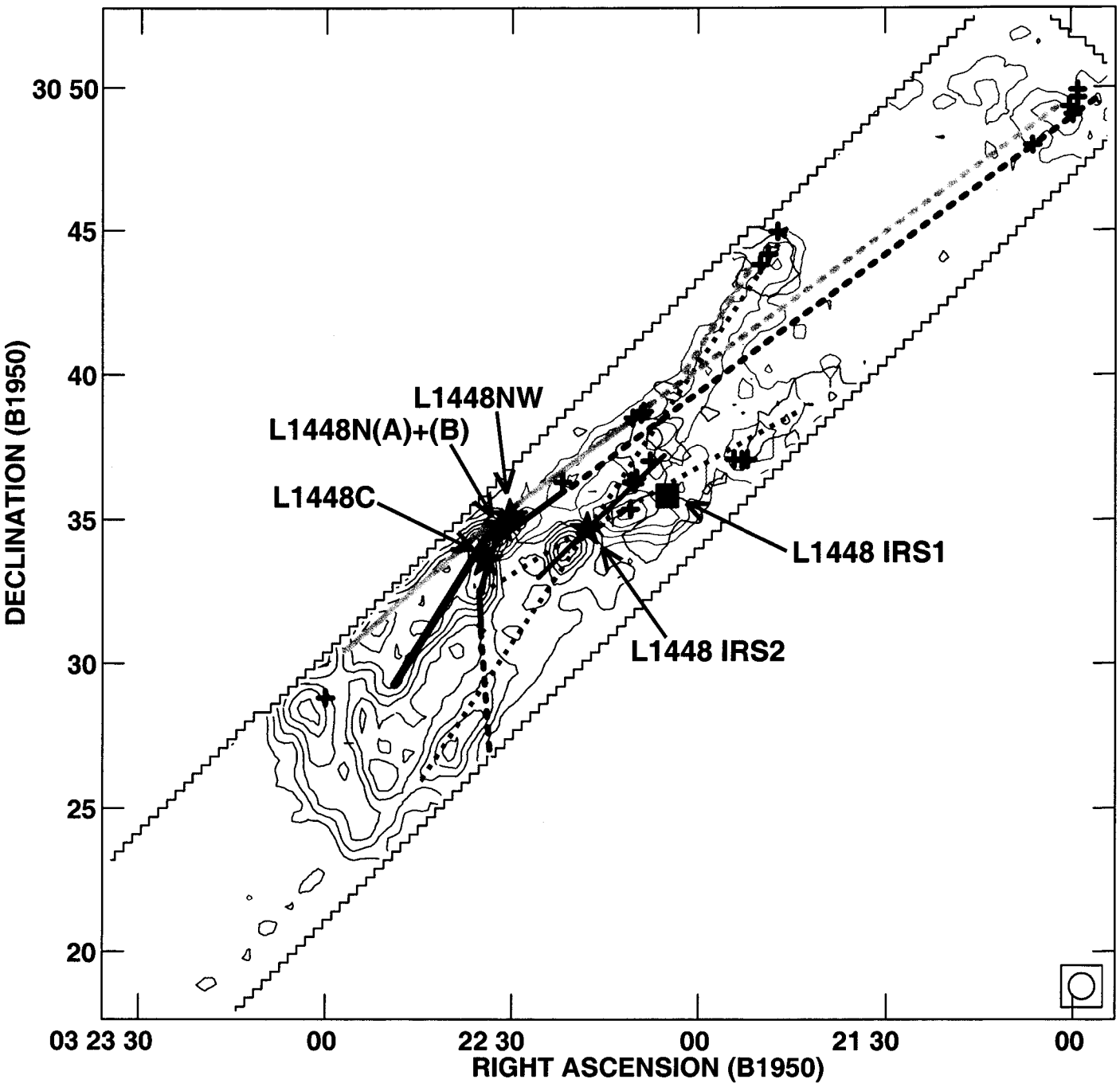
30 50
45
40
35
30
25
20
DECLINATION (B1950)
L1448NW
L1448N(A)+(B)
L1448C
L1448 IRS1
L1448 IRS2
03 23 30
00
22 30
00
21 30
00
RIGHT ASCENSION (B1950)

Fig 6

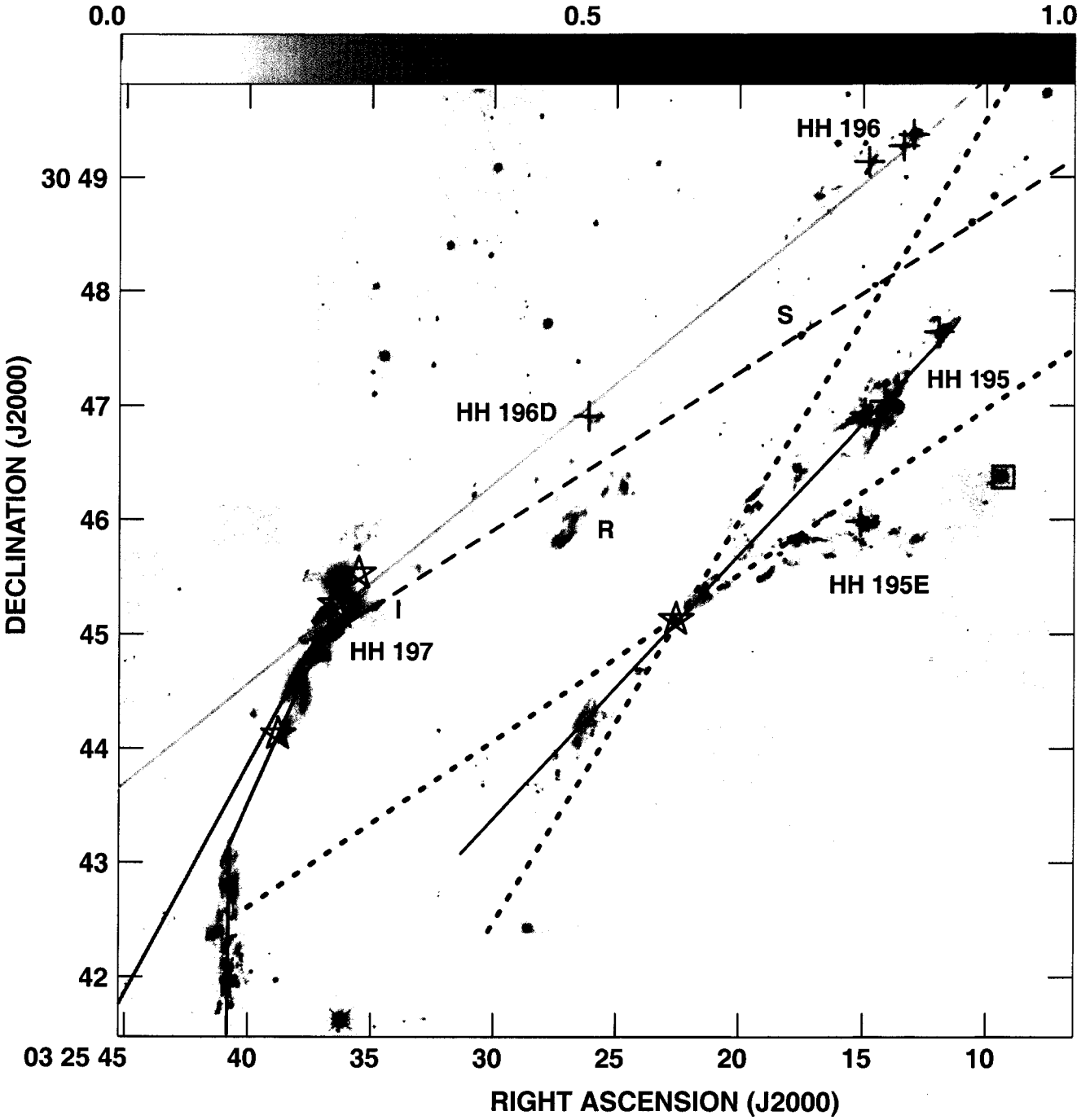
0.0
0.5
1.0
HH 196
30 49
48
S
HH 195
47
HH 196D
46
R
HH 195E
I
45
HH 197
44
43
42
DECLINATION (J2000)
03 25 45
40
35
30
25
20
15
10
RIGHT ASCENSION (J2000)

Fig 7